[1]R. E. Trees, Phys. Rev. 92, 308 (1953); C. Schwartz, *ibid.* 97, 380 (1955).
[2]R. K. Nesbet, Phys. Rev. A 2, 661 (1970).
[3]B. N. Taylor, W. H. Parker, and D. N. Langenberg, Rev. Mod. Phys. 41, 375 (1969).
[4]N. F. Ramsey, *Molecular Beams* (Oxford U. P., New York, 1956), p. 172.
[5]*Handbook of Chemistry and Physics* (Chemical Rubber, Cleveland, 1969), 49th edition.
[6]R. K. Nesbet, Proc. Roy. Soc. (London) A230, 312 (1955).
[7]A. Abragam and M. H. L. Pryce, Proc. Roy. Soc. (London) A205, 135 (1951).
[8]D. R. Hartree, *The Calculation of Atomic Structures* (Wiley, New York, 1957).
[9]J. D. Lyons, R. T. Pu, and T. P. Das, Phys. Rev. 178, 103 (1969); 186, 266 (1969).
[10]D. A. Goodings, Phys. Rev. 123, 1706 (1961).
[11]W. A. Goddard III, Phys. Rev. 182, 48 (1969).
[12]H. F. Schaefer III, R. A. Klemm, and F. E. Harris, Phys. Rev. 176, 49 (1968).
[13]R. K. Nesbet, Phys. Rev. 155, 51 (1967); 155, 56 (1967); 175, 2 (1968); Advan. Chem. Phys. 14, 1 (1969).
[14]K. A. Brueckner, Phys. Rev. 96, 508 (1954); 97, 1353 (1955); 100, 36 (1955); in *The Many-Body Problem*, edited by B. deWitt (Wiley, New York, 1959), pp. 47–241.
[15]R. K. Nesbet, in *Quantum Theory of Atoms, Molecules, and the Solid State*, edited by P.-O. Löwdin (Academic, New York, 1966), pp. 157–165; Colloq. Intern. Centre Natl. Rech. Sci. (Paris) 164, 87 (1967).
[16]H. F. Schaefer III and F. E. Harris, Phys. Rev. 167, 67 (1968).
[17]H. F. Schaefer III and U. Kaldor, J. Chem. Phys. 49, 468 (1968).
[18]E. Clementi, C. C. J. Roothaan, and M. Yoshimine, Phys. Rev. 127, 1618 (1962).
[19]D. R. Hartree, *Numerical Analysis* (Oxford U. P., New York, 1952), pp. 196–197.
[20]L. C. Gomes, J. D. Walecka, and V. F. Weisskopf, Ann. Phys. (N.Y.) 3, 241 (1958).

PHYSICAL REVIEW A VOLUME 2, NUMBER 4 OCTOBER 1970

Level-Crossing Measurement of Lifetime and hfs Constants of the $^2P_{3/2}$ States of the Stable Alkali Atoms*

Robert W. Schmieder† and Allen Lurio
IBM Watson Laboratory, Columbia University, New York, New York, 10025
and
W. Happer and A. Khadjavi
Columbia University, New York, New York 10027
(Received 27 February 1970)

Measurements have been made of the hyperfine structure (hfs) constants and lifetimes of the first and second $^2P_{3/2}$ states of the stable alkali atoms, except lithium, using the pure magnetic field level-crossing technique. The results for Na^{23} are

State	a (MHz)	b (MHz)	τ (nsec)
$3^2P_{3/2}$	18.9±0.3	2.4±0.3	16.0±0.5
$4^2P_{3/2}$	6.2±0.2	1.0±0.1	95 ±4

The results for K^{39} have been reported previously. For Rb^{85} and Cs^{133}, hfs constants were obtained that agreed with, but were less accurate than, previous work. The measured lifetimes are

Element	State	τ (nsec)
Rb^{85}	$5^2P_{3/2}$	25.5±0.5
	$6^2P_{3/2}$	118 ±4
Cs^{133}	$6^2P_{3/2}$	32.7±1.5
	$7^2P_{3/2}$	134.5±2.8

The error limits in these measurements are two standard deviations. The above results were obtained by fitting the observed level-crossing signal to a theoretical line shape computed from the Breit formula, using a, b, and τ as parameters.

I. INTRODUCTION

The stable alkali atoms continue to be the objects of widespread theoretical and experimental study. Their importance stems from their utility as frequency standards[1] and magnetometers,[2] as probes of interaction processes such as atom-atom collisions[3] and new effects such as light-

induced level shifts,[4] and as tests of atomic structure calculations.[5] The ground states of these atoms have been carefully studied, and many ground-state properties, such as magnetic moments and hfs, are very accurately known. The excited states, on the other hand, are considerably more difficult to study experimentally, mainly because the natural width obscures the detailed structure of these states. Serious gaps and inconsistencies have existed in the available data,[6] and we therefore undertook a series of measurements aimed at improving our knowledge of these states. Our work was directed at measuring lifetimes, hfs constants, and static electric polarizabilities of the $^2P_{3/2}$ states. Although many of these measurements have been carried out previously in other laboratories, we felt that a set of measurements from one laboratory, using essentially the same apparatus on all the alkalis, would be valuable. We used the level-crossing technique with pure magnetic or electric field.

This paper describes the pure magnetic field measurements and the results derived therefrom. Results include the lifetimes of the first and second $^2P_{3/2}$ states of Na, K, Rb, and Cs, and the hfs constants of the first and second $^2P_{3/2}$ states of Na^{23} and K^{39}. The results for K^{39} have already been reported.[7] No results for lithium are included here because lithium vapor presents special handling problems and the work is still in progress in this laboratory. The results of the pure electric field level-crossing work is reported in two separate papers.[8,9] Further details of this work are available in a separate report.[10]

II. EXPERIMENTAL METHOD

Figure 1 shows the experimental geometry. Light from the resonance lamp is plane polarized and focused (with lenses not shown) onto a beam

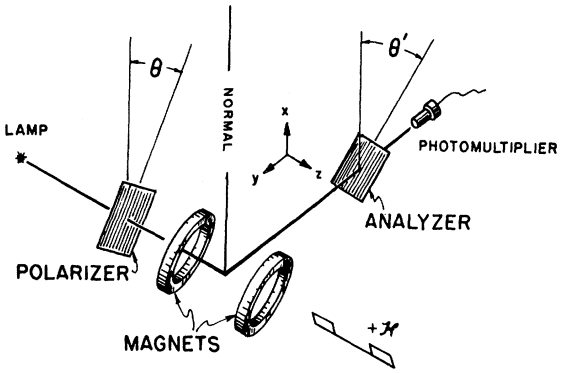

FIG. 1. Schematic diagram of experimental geometry. The angles θ and θ' used in text are indicated.

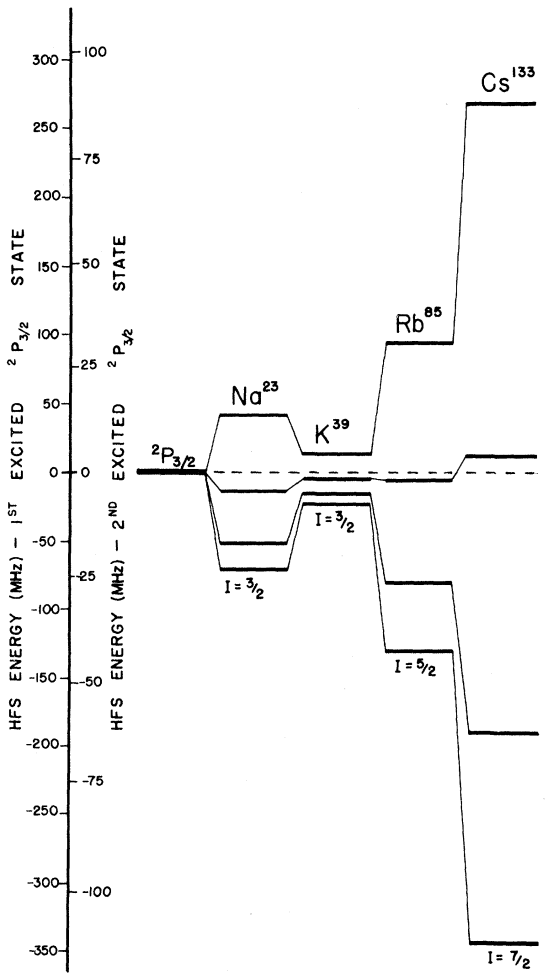

FIG. 2. Relative spacing of the hyperfine energy levels of the stable alkali atoms.

of free atoms. The resonantly scattered light is collected and passed through an analyzer to a photomultiplier. A slowly varying uniform magnetic field is applied to the atoms with Helmholtz coils.

When the field is zero, the $^2P_{3/2}$ states are split into four hyperfine states of total angular momentum $F = I + \frac{3}{2}$, $I + \frac{1}{2}$, $I - \frac{1}{2}$, $I - \frac{3}{2}$, where I is the nuclear spin. Figure 2 shows the relative spacing of these levels for Na^{23}, K^{39}, Rb^{85}, and Cs^{133}. The three intervals for each case are adequately specified by two interaction constants a, b, the dipole and quadrupole hfs constants. As the field is increased from zero, the F states are split into their magnetic substates, some of which may cross others. If the condition $|\Delta m| \leq 2$ is satisfied, where Δm is the difference in magnetic quantum numbers of the crossing levels, then it is possible to detect the crossing by its effect on

the scattered light. When scattered light of a particular polarization is detected from a particular direction, the effect is an increase or decrease in the measured intensity. Plotting intensity versus field thus results in a characteristic line shape that depends on the hfs constants and the natural width (reciprocal of the mean lifetime τ), as well as on the polarizer-analyzer orientations and the details of the energy levels near the crossings. The object of our measurements was the extraction of a, b, and τ from the observed line shapes.

III. THEORY OF LINE SHAPE

The shape of the fluorescent intensity versus magnetic field can be calculated accurately with the Breit formula[11]

$$S = C \sum_{\mu\mu',mm'} \frac{\langle \mu | \hat{e} \cdot \vec{p} | m \rangle \langle m | \hat{e}^* \cdot \vec{p} | \mu' \rangle \langle \mu' | \hat{e}' \cdot \vec{p} | m' \rangle \langle m' | \hat{e}'^* \cdot \vec{p} | \mu \rangle}{\frac{1}{2}(\Gamma_\mu + \Gamma_{\mu'}) + i(E_\mu - E_{\mu'})/\hbar} , \tag{1}$$

where C is a constant that depends on the experimental geometry; $\vec{p}$ is the electric dipole moment operator; $\hat{e}$, $\hat{e}'$ are the polarization vectors of the incident and scattered light; μ, μ' indicate two intermediate substates; m, m' indicate the initial and final substates; and E and Γ are the energy and natural width of the intermediate states. Equation (1) is valid if (i) the spectral profile of the incident light is uniform over the absorption profile of the fluorescing atoms; (ii) the intensity of the incident light is weak (i.e., the excitation rate is small compared to the decay rate).

The numerical calculations of S were performed with a FORTRAN IV program which operates in two main steps. First, it diagonalizes[12] the operator representing the hfs and magnetic field perturbations

$$V = a\vec{I} \cdot \vec{J} + b \left(\frac{3(\vec{I} \cdot \vec{J})^2 + \frac{3}{2}(\vec{I} \cdot \vec{J}) - I(I+1)J(J+1)}{2I(2I-1)J(2J-1)} \right)$$
$$+ g_I \mu_0 \vec{\mathcal{H}} \cdot \vec{I} + g_J \mu_0 \vec{\mathcal{H}} \cdot \vec{J} , \tag{2}$$

where $\mathcal{H}$ is the magnetic field (normally assumed in the z direction), and g_I, g_J are the (known) g factors. The diagonalization yields the energy eigenvalues E_μ, $E_{\mu'}$ and the eigenvectors $|\mu\rangle$, $|\mu'\rangle$, etc., of the excited substates. Second, these quantities are used in Eq. (1) to compute the scattered intensity.

The outputs of the program are (i) the energy levels for a range of field values and (ii) the corresponding values of the scattered intensity. These data are plotted on a Stromberg-Carlson 4929 CRT plotter, which generated a 9 × 9-in. graph, accurate to one part in 1024. Computation time for a typical set of curves is a few min and plotting time is a few sec. With this system we could compute predicted line shapes for a large variety of experimental conditions and examine the effect of varying a single parameter on the observations.

In Fig. 3, we present the results of a typical computation. It shows the predicted line shape for polarizer-analyzer orientations $(\theta = 90°)/(\theta' = 0°)$ for the $5^2P_{3/2}$ state of Rb^{85}, as determined from Eq. (2).

IV. APPARATUS

The apparatus can be divided conveniently into three parts: (i) experimental section (Sec. IV A); (ii) electronics (Sec. IV B); (iii) data storage and readout (Sec. IV C). The apparatus was improved during the course of this work; most of the descriptions apply to the later configurations.

A. Experimental Section

The experimental section consists of a large rigid aluminum frame with brackets for mounting

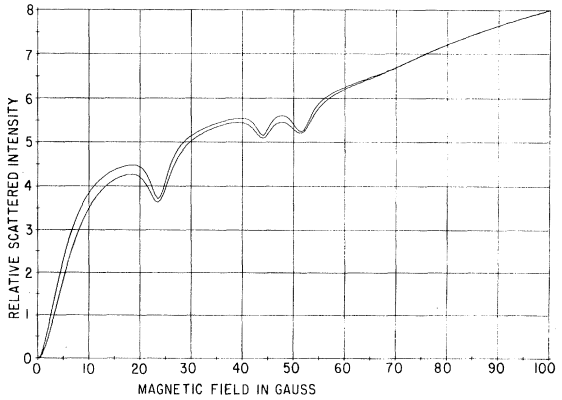

FIG. 3. Theoretical level-crossing curve computed for the $5\ ^2P_{3/2}$ state of Rb^{85} for two different values of the lifetime τ and $\theta/\theta' = 90°/0°$. The input data are $J = \frac{3}{2}$, $I = \frac{5}{2}$, $g_J = \frac{4}{3}$, $g_I = -0.000\ 293$, $\tau = 26$ and 30 nsec, $a = 25.029$ MHz, and $b = 26.032$ MHz.

various coils, vacuum system, etc. The entire structure is nonmagnetic. There are two pairs of large Helmholtz coils for cancelling the earth's magnetic field, one with its axis vertical, the other with its axis horizontal. The scattering of the light occurred at the centers of these coils. The third component of the field was not cancelled, and was about 125 mG in a direction parallel to the applied magnetic field in the z direction.

The scattering occurred in a chamber about 3 in. diam and 15 in. high. Figure 4 shows an elevation cross section of this chamber.

The atomic beam is produced in the lower part of the chamber by an electrically heated stainless-steel oven and a series of collimators. The metal evaporates through a crinkle-foil plug, is collimated, passes through the scattering region, and is frozen onto a liquid-nitrogen-cooled trap in the upper portion of the chamber. The oven was kept at a temperature such that the vapor pressure of the metal was between 10^{-2} and 5×10^{-2} mm Hg. In order to avoid scattering of the atomic beam in the chamber, pressures of less than 10^{-6} mm Hg were maintained in all experiments.

The z-axis magnetic field was produced by a pair of 15-in.-diam Helmholtz coils. The coils were calibrated with a rubidium magnetometer and found to produce 14.09 G/A at their center. For some measurements, smaller Helmholtz coils, producing 6.93 G/A at their center, were used. One of these two coils was usually used to provide a small negative offset field while the other was swept in a triangular cycle. The offset field was subtracted off in the analysis. When measuring high-field crossings, one set of coils provided a large positive offset field, while the others swept over a small range around that offset.

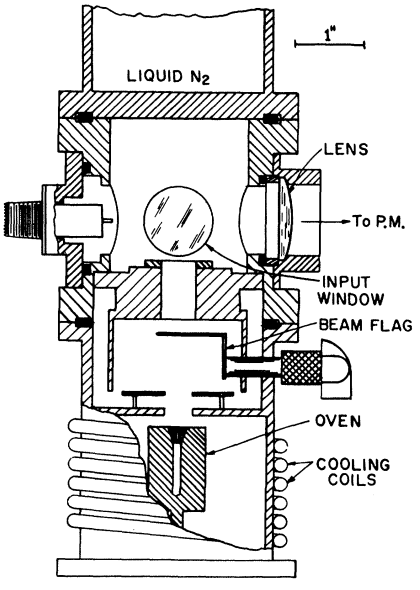

FIG. 4. Scattering chamber for magnetic field measurements. The light enters from the window at the rear. The light scattered by the atomic beam is collected by the lens on the right and focused through a light pipe into the photomultiplier. Details of the N_2 trap are not shown.

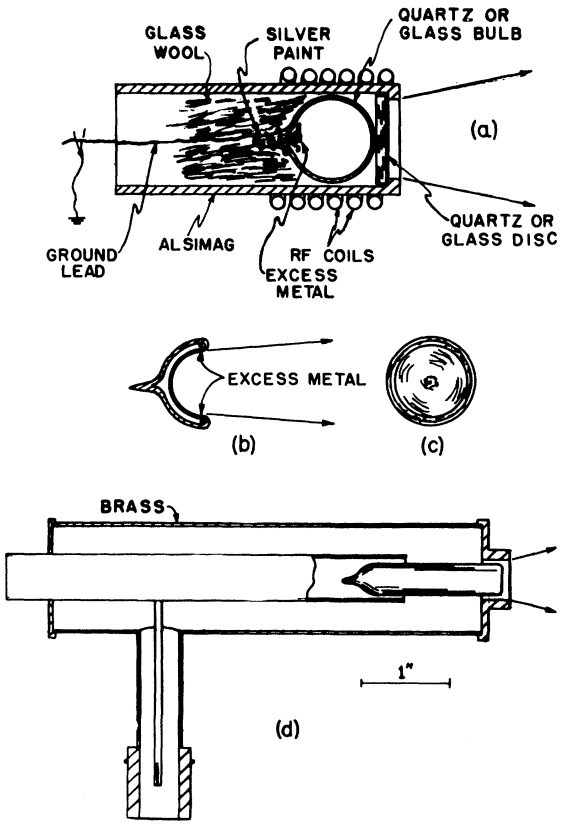

FIG. 5. Typical lamps used in the work; see text for description.

The incident light (from a resonance lamp located 15–30 in. away from the beam) was focused by one or more lenses into a region about $\frac{1}{2}$ in. diam. The region of the scattering was limited to the area where the field is uniform. Sometimes stops or a diaphragm, or both were used to improve the focus at the expense of total intensity. Quartz lenses and windows were used throughout.

A wide variety of light sources was used during the course of this work. Most of these lamps were electrodeless glass or quartz bulbs containing a small amount of alkali metal and excited by rf or microwave power. Figure 5 shows some typical lamps we used. The light output of our lamps was generally comparable to, or better than, the Osram-type lamps (which we occasionally

used), although our lamps were not uniformly reliable.

Figure 5(a) shows one arrangement we used successfully. It consists of a glass bulb about $\frac{3}{4}$ in. diam, held in a heat insulating mount, and both excited and heated by 14-MHz rf power. The lamp must be hot enough to maintain reasonable vapor pressure in the bulb, but too much rf power creates hot spots and burns a small hole in the bulb. Normally, the lamps were made with a few mm Hg of a noble gas (Ar, He, Kr) as a buffer. The color of the light emitted by these lamps was due in part to the emission by the buffer gas. It was found that a ground connection significantly increased the brightness of the discharge. The connection was in the form of a heavy copper wire cemented around the stem of the lamp with silver paint. Many variations of this arrangement were used, but there seemed to be no optimum arrangement for all lamps.

Figure 5(b) shows a modification of the usual lamp, used mainly for the first resonance lines. The bulb is pulled inward when it is made, forming a concave front. The excess metal collects in a ring around the front. These lamps were designed to reduce self-reversal in the first resonance lines. They sometimes exhibited an instability that was not present with other geometries: Often they would form a radial pattern of bright spots [see Fig. 5(c)] and the pattern as a whole would rotate around the axis of the lamp at a rate dependent upon the rf excitation power. In spite of these difficulties, we were able to get these lamps to stabilize, and they operated well for long periods of time.

Figure 5(d) shows a simpler lamp operated in a microwave cavity. The lamps were made from pyrex or quartz, and were viewed (by the apparatus) from the flattened end. These lamps were excited by a Raytheon PGM10X1 2450-MHz generator and were among the most stable of any we tried. Various combinations of tuning stubs, lamp sizes, etc., were tried, but again no general conclusion was reached about optimizing the output power. The variations among this type of lamp were not nearly so marked as with other types.

One of the main problems with these electrodeless lamps was the decrease of the output power because of the alkali metal reacting with the glass or quartz. The reaction causes a darkening of the lamp and serious absorption of the light. The rate of deterioration increases rapidly with increased power input and many of the lamps lasted only a few hours. The reaction can be partially reversed by heating the lamp carefully with a flame, but this is generally more difficult than making a new one. We found that Na and K darkened quartz much faster than Pyrex, and that Corning 1720 glass was slower in darkening than pyrex. However, the 1720 glass is almost opaque below 4000 Å, so is of no use in the near ultraviolet.

We have recently made some effort at retarding the darkening of these lamps. The general idea is to saturate the inside surface with alkali atoms by heating the lamp carefully with an alkali salt inside. The alkali ions presumably move into the glass surface and form a saturated solution but do not react to darken the glass. When the finished lamp, containing the same alkali metal, is excited, the free alkali-metal atoms diffuse into the glass much more slowly. Thus, color-center formation is retarded and the lamp lasts longer. We have tested several lamps made this way and found that they did indeed operate longer with more excitation than uncoated lamps. However, the tests were not extensive and we cannot say to what extent this technique will be of value.

The light from the lamp passes through polaroid polarizers on the way into and out of the scattering chamber (Fig. 4). In all the measurements reported here, plane polarized light was used. Interference filters with transmission half-width of about 50 Å were used in the output end of the scattering chamber, and sometimes a broadband glass filter was used on the input side to further reduce unwanted light.

The scattered light was collected by an $f/2$ lens and passed down a 1-m light pipe, constructed by aluminizing the inside surface of a glass tube and mounting it in a brass tube.

The photomultiplier was located at the end of the light pipe in a Jarrell-Ash thermoelectric cooler. The cooling was not needed for the Amperex 56UVP tube, since the dark current for near-uv tubes is not nearly as serious a problem as for near-ir tubes.

A flag attached to a vacuum feed-through enables the experimenter to mechanically block the beam in order to estimate the amount of scattering from the beam in relation to the background.

B. Electronics

A block diagram of the electronics is shown in Ref. 7. The averager, translator, plotter, and card punch are described in Sec. IV C.

The magnetic field was swept in a triangular wave of 16-sec period. This sweep was controlled by a low-frequency function generator which fed a current-regulated supply used to drive the coils. The field was measured by monitoring the current through a precision resistor in series with the coil. Any nonlinearities in the sweep

were accounted for by storing the field (i.e., current) versus time and then combining with the intensity versus time signal to obtain intensity versus field. The function generator provided a pulse at the peak of each cycle which was used to synchronize the signal averager with the phase of the sweep.

C. Data Storage and Readout

The signal-to-noise (S/N) ratio of the data was significantly increased by the use of a signal averager or CAT, an acronym for computer of average transients. If n sweeps are made, the S/N ratio is multiplied by $\sqrt{n}$.

The signal from the photomultiplier was amplified to about 3-V peak and fed directly into the CAT input. The CAT converts it into digital form by a frequency-modulated oscillator followed by a counter and a 1024 address memory. Each address stores a 6-digit number in 24-line BCD form (4 bits per decimal digit). The addresses are interrogated sequentially during the 16-sec sweep so the entire signal versus time is stored across the 1024 channel memory. The linearity of analog-to-digital conversion is better than 0.1%.

The CAT has both an analog and a digital readout mode. The analog output was connected directly to an x-y plotter to provide a permanent record of the raw experimental data. The digital output was fed through a BCD-decimal translator that formed the interface to a modified IBM model 526 card punch. The output format was fixed as 10 addresses per card. It takes about $7\frac{1}{2}$ min to unload the entire 1024 channel memory onto 103 cards. In more recent experiments, an interface was designed to read the entire CAT memory directly into an IBM 1130 computer in about 3 sec.

V. EXPERIMENTAL PROCEDURE

The alkali metals were obtained from A. D. MacKay & Co., New York, N. Y., in sealed glass vials $\frac{1}{4}$ in. diam. About $\frac{1}{2}$ g of the metal in the opened vial was placed in the oven, the chamber was evacuated, and the oven was heated to form the beam. Scattering by the beam was detected by operating the beam blocking flag. Data accumulation was continued as long as the appartus was stable, which ranged from 30 min to many hours. At the end of the accumulation, the data was read out, and a field calibration sweep was taken and read out.

VI. ANALYSIS OF DATA

The data (on punch cards) was first preprocessed by an IBM 1620 program that checks for errors and then adds the symmetrical halves (generated by the triangular sweep) together. The latter operation eliminates unidirectional drifts caused by lamp deterioration, beam change, etc. The data were then compared with theoretical data generated with assumed values of a, b, and τ. This program also computes the mean-square deviation (MSD) of the experimental data from the theoretical data, and in a series of such computation for various values of a, b, and τ, one set of values will give the minimum MSD. This set of values is considered to be the result of the measurements.

The statistical error was determined from the plot of MSD versus a, b, or τ. The error limits quoted in the results represent two standard deviations.

In determining the values of several parameters from one set of experimental data, it is necessary to assume that the best fit is unique – that is, no other set of values of the parameters would give as good a fit. In our measurements, the convergence of multiple parameters to best values was rapid, stable, and so far as we can tell, unique.

VII. EXPERIMENTAL DATA

Figures 6(a) and 6(b) show some typical experimental line shapes observed with our apparatus. All these curves were taken with the polarizer orientation $\theta = 90°$ and the analyzer orientation

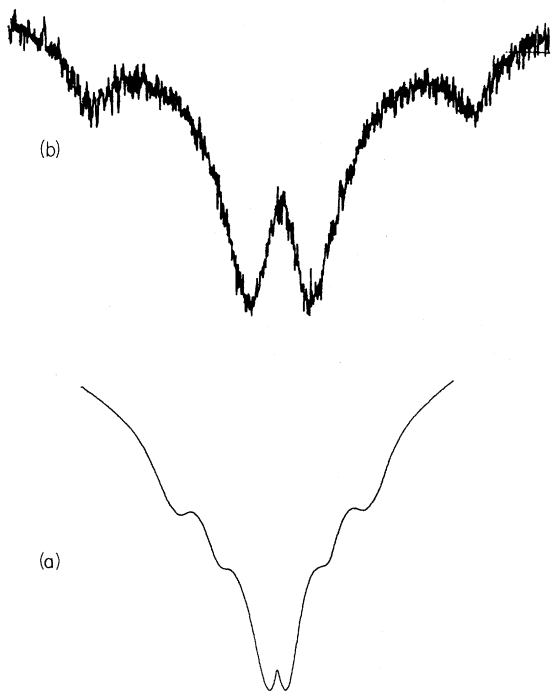

FIG. 6. Typical experimental data as read out from the averager on an x-y plotter. (a) $Na^{23}\,3^2P_{3/2}$, (b) $Na^{23}\,4^2P_{3/2}$.

$\theta = 0°$ (see, for example, Fig. 1). They are roughly symmetrical around their centers due to the triangular sweep of the field. From left to right in these plots, the field drops from a large positive value through zero to a small negative value, then back up through zero to a large positive value. A good indication of the stability of the apparatus is the actual symmetry of the data. These curves were drawn by the x-y plotter and appear continuous, although they actually consist of 1024 separate points. The curves in Fig. 6 show how overlap of high field crossings with the Hanle effect seriously complicates the line shape.

Figure 7 shows a Cs^{133} $7\,^2P_{3/2}$ signal taken under slightly different conditions. The field was swept over a range of about 49 G with an 8-G offset to show the symmetrical Hanle effect around zero field and the first high-field crossing. In the measurements taken to determine the lifetimes of Cs and Rb, the field was swept only over the narrow range of this first high-field crossing. The reason for using this crossing is explained in Sec. IX. We also made sweeps over the double crossings in Rb and Cs (see, for example, Fig. 3); the results were reasonably consistent with the single-crossing data.

In Figs. 8 and 9, we have plotted a single set of experimental data for each of the first two $^2P_{3/2}$ states of Na^{23}, Rb^{85}, and Cs^{133}, and the theoretical line shape calculated for the best set of parameters (a, b, τ). The best set (a, b, τ) was found as the weighted average of the optimum set found for each independent measurement of a given state. The numerical values quoted as results were obtained as the average of several runs, of which only a single run is presented here. The numbers showed good agreement from run to run.

VIII. RESULTS OF MEASUREMENTS

A. Lifetimes

Table I lists the final values of the lifetimes we obtained from our data. These values are the weighted averages of multiple independent measurements. The error limits in Table I represent two standard deviations. For completeness, we have included the results for K^{39}, already reported in Ref. 7. A complete list of our individual measurements and a compilation of theoretical and experimental lifetimes appearing through 1968 are given in Ref. 10.

We also computed the lifetimes with a program that uses the Bates-Damgaard method[13] to generate the radial integrals, rather than the tables given by these authors. Direct computation was the technique used by Heavens,[14] and our results agreed with his to within 1%.

B. hfs Constants

In Table II, we list the values of the hfs constants a, b for Na^{23} and K^{39} resulting from our experimental data. The remarks pertaining to Table I apply here. The a and b values for K^{39} are discussed in Ref. 7. We do not list values for Rb or Cs because our experiments confirmed the results of others but did not materially improve their accuracy. A list of the individual measurements and a complete list of theoretical and experimental results for stable alkalis through 1968 are given in Ref. 10.

C. Other Results

1. *Nuclear Electric Quadrupole Moments*

The ratio of the hfs constants b/a can be used to estimate the value of the nuclear electric quadrupole moment Q, if the nuclear magnetic dipole moment μ is known, since Q is proportional to b/a. A discussion of this relationship is given by Kopfermann.[15] Using the average of b/a in the first and second states, the data in Table II give

$$Q(Na^{23}) = (0.095 \pm 0.02) \times 10^{-24}\ \text{cm}^2,$$

$$Q(K^{39}) = (0.056 \pm 0.003) \times 10^{-24}\ \text{cm}^2.$$

These values are slightly smaller than most previous measurements, although they may not be significantly smaller. In the case of K^{39}, our result has been confirmed by three recent experi-

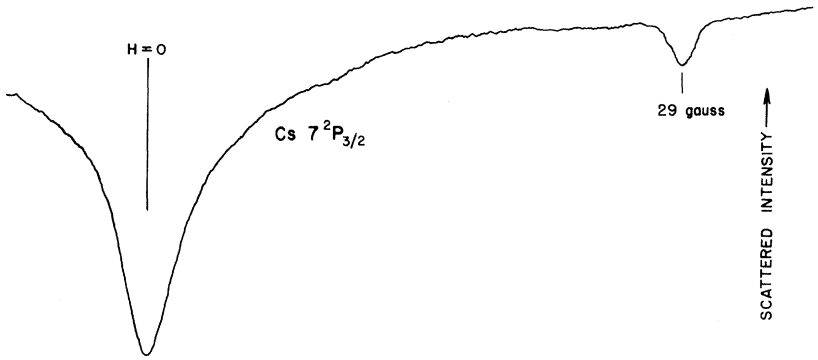

FIG. 7. Typical experimental data for Cs^{133} $7^2P_{3/2}$ showing the Hanle effect at $\mathcal{H} = 0$ and a single crossing at $\mathcal{H} = 29$ G. There is a pair of crossings at higher field similiar to those seen in Fig. 3.

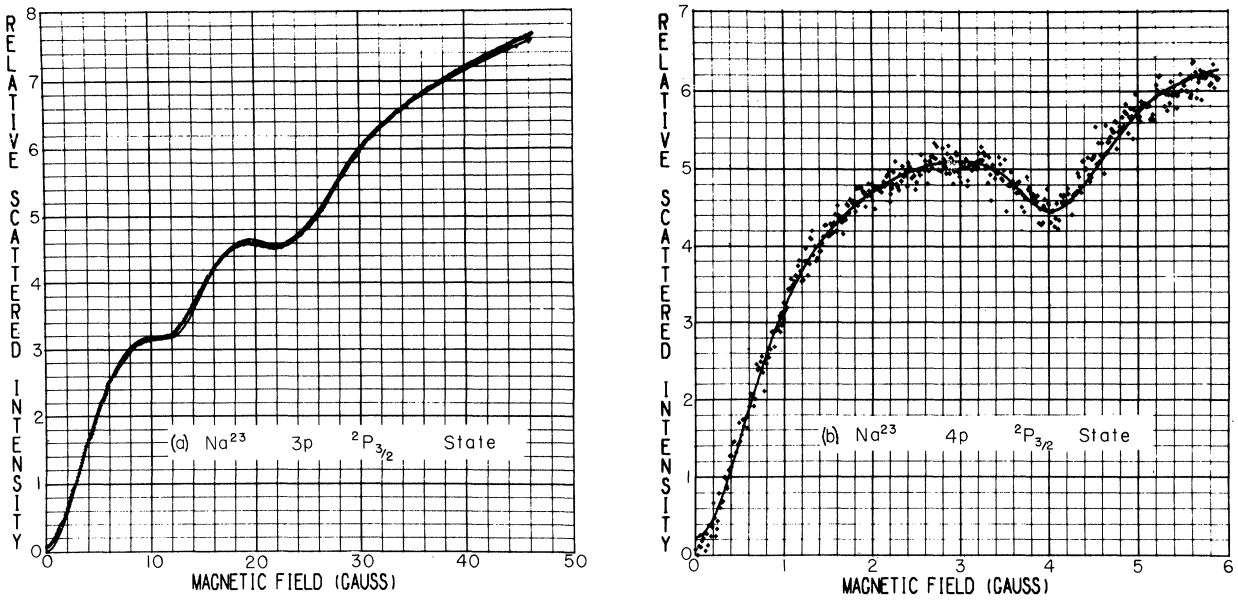

FIG. 8. Experimental data and one of the best-fit theoretical curves for (a) $Na^{23}\,3^2P_{3/2}$, (b) $Na^{23}\,4^2P_{3/2}$.

ments.[16] The above values do not include Sternheimer corrections,[17] since the errors in the corrections are somewhat larger than the errors in our results.

2. *Scaling of the* hfs *Constants*

It is well known[15] that (a) the hfs constants a, b are predicted to be proportional to the fine-structure (fs) intervals and (b) that we have

$$a(n^2P_{1/2})/a(n^2P_{3/2}) = 5F_r(\tfrac{1}{2}, Z_i)/F_r(\tfrac{3}{2}, Z_i),$$

where the F_r are relativistic correction factors. In order to test these relations, we used published data including our new results on Na^{23} and K^{39} to compute ratios of a, b in adjacent fs doublets. Table III shows these ratios for the $^2P_{3/2}$ states, and the ratios of the fs separations as listed in Moore's tables.[18] These results are evidence that $a(n^2P_{3/2})$ is indeed proportional to the fs, although there may be some significant discrepancies in this table. The observed ratios of $b(n^2P_{3/2})$ do not agree with the fs ratios as dramatically, but this circumstance is probably due to larger errors in the measured values of b.

The relationship

$$a(n^2P_{1/2})/a(n^2P_{3/2}) = 5F_r(\tfrac{1}{2}, Z_i)/F_r(\tfrac{3}{2}, Z_i)$$

is known to be less reliable, as can be seen in Table IV where we use our measurements, the values of Table II, and other published work. The discrepancy in the lithium ratio is known to be due to core polarization[5] but no definite explanation is yet available for the discrepancies in the other ratios, although zu Pultlitz[19] has mentioned that the spin-orbit interaction may perturb the hfs, as originally suggested by Fermi.[20]

TABLE I. Results of the lifetime measurements.

Element	State	Lifetime (nsec)
Na	$3^2P_{3/2}$	16.0±0.5
	$4^2P_{3/2}$	95 ±4
K	$4^2P_{3/2}$	26.0±0.5
	$5^2P_{3/2}$	140.8±1.0
Rb	$5^2P_{3/2}$	25.5±0.5
	$6^2P_{3/2}$	118 ±4
Cs	$6^2P_{3/2}$	32.7±1.5
	$7^2P_{3/2}$	134.5±2.8

IX. DISCUSSION

In analyzing our data we ignored a number of potentially important effects. We list some of these and briefly indicate why they should be negligible.

A. $^2P_{1/2}$ States

In all our measurements except the first excited states of Rb and Cs, the $^2P_{1/2}$ light was not rejected by the interference filter. However, it has been shown[21] that excitation from a $J=\frac{1}{2}$ state to another $J=\frac{1}{2}$ state using linearly polarized light will not give rise to any level-crossing signal.

B. Multiple Isotopes

Only natural stable isotopes were used in these experiments, which means that a mixture of iso-

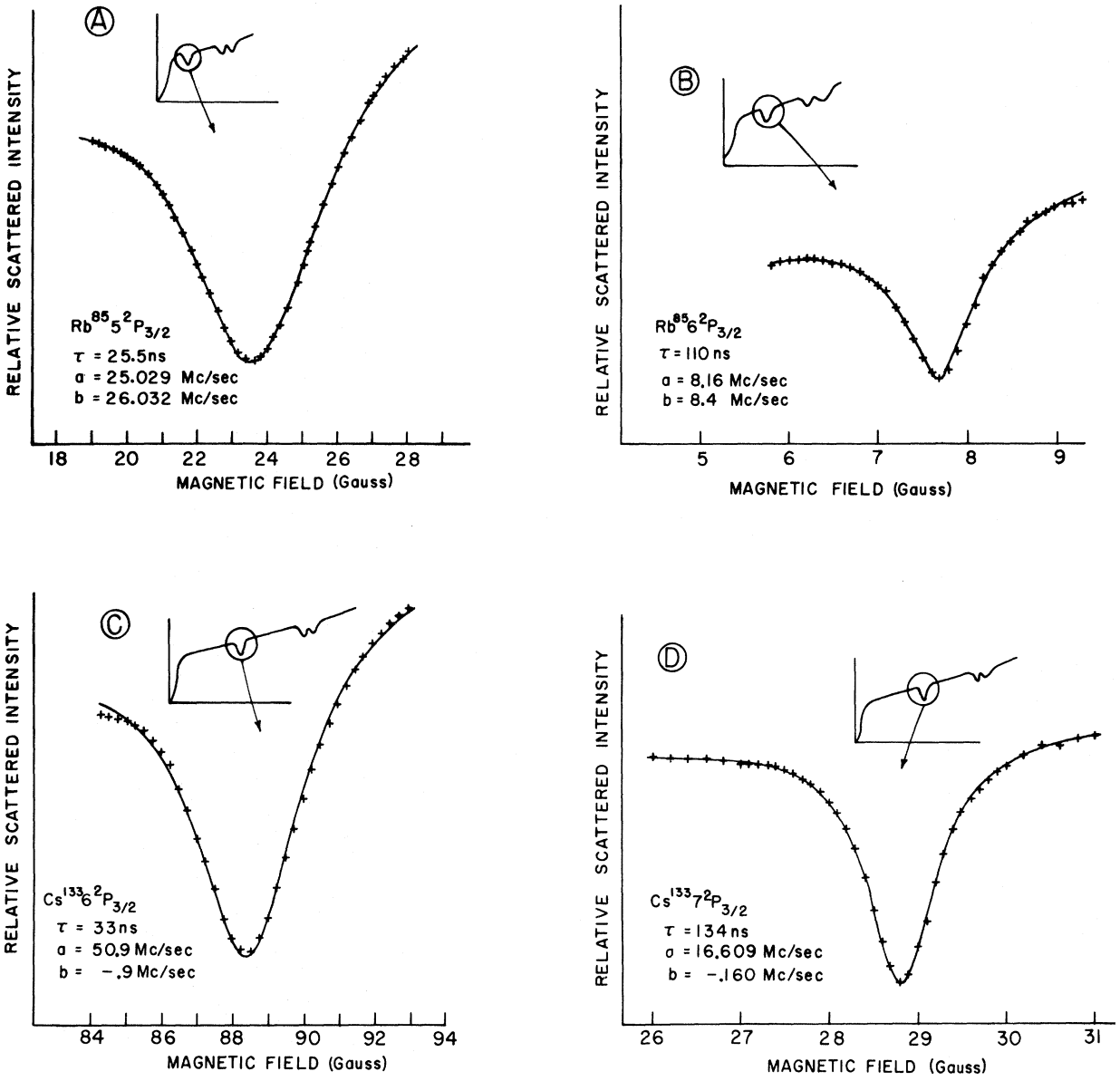

FIG. 9. Experimental and best-fit theoretical curves for the first and second $^2P_{3/2}$ states of Rb^{85} and Cs^{133}. The range of the magnetic field is identified by the insets.

topes was present. The problem is most acute in Rb, where Rb^{87} is almost 30% of the total. Since the hfs in different isotopes is different, the level-crossing signals will be different. To show the effect, we plot (Fig. 10) the signals for Rb^{85} and Rb^{87} in the $6\,^2P_{3/2}$ state, using $\theta = 90°$, $\theta' = 0°$. In this plot, the vertical scales for both curves are the same, but the curves have been displaced vertically to coincide at $\mathcal{H} = 0$. The expected experimental signal would be the sum of these curves, each times its respective abundance.

In addition, the size of the hfs in Cs and Rb is large enough that one cannot assume each hfs level of a given isotope is excited with the same intensity. Thus, the relative sizes of the observed zero- and high-field level-crossing signals in a single isotope may not be the same as those shown in Fig. 10, where a uniform profile was assumed. Actually, since we used natural Rb in both the lamp and the beam, the contribution of the Rb^{87} to the signal will be somewhat less.

The important fact shown in Fig. 10 is that the single crossing in Rb^{85} near 8 G occurs at a relatively flat region in the Rb^{87} signal. Thus, there should be small distortion of the Rb^{85} signal over the region of that crossing, when natural Rb is

TABLE II. Results of the hfs constants measurements.

Element	State	a(MHz)	b(MHz)
Na^{23}	$3^2P_{3/2}$	18.9 ±0.3	2.4 ±0.3
	$4^2P_{3/2}$	6.2 ±0.2	1.0 ±0.1
K^{39}	$4^2P_{3/2}$	6.0 ±0.1	2.9 ±0.2
	$5^2P_{3/2}$	1.95 ± 0.05	0.92 ±0.1

used, and the distortion that does occur will be very nearly a linear function of $\mathcal{H}$. In order to compensate for this linear distortion, we included in the fitting program the facility for adding a sloping baseline to the theoretical or experimental data, and adjusted the slope to give the best fit. The magnitudes of the slopes thus determined were consistently small, and the best-fit lifetime τ was not highly sensitive to this slope. Thus, we are reasonably confident that the presence of Rb^{87} did not materially affect the measured lifetime.

C. Spectral Profile of Lamp

The Breit formula, which was used in all the calculations of scattered intensity, assumes a white-light source. This requirement is imposed in the step when the expression for monochromatic scattering is integrated over all incident frequencies. It is a good approximation in most cases.

The broad-profile criterion will be much better satisfied for Na and K than for Rb and Cs for two reasons: (i) The Doppler width of the lamps will be larger for the lighter atoms; (ii) the hfs in the lighter atoms is much smaller. Consequently, we would expect better fits of the (Breit formula) theoretical curves to the experimental data, and this has been borne out.

We made no profile corrections in analyzing the

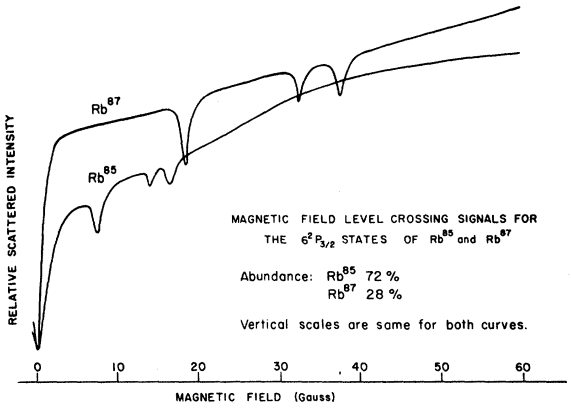

FIG. 10. Theoretical level-crossing signals for the $6\,^2P_{3/2}$ states of Rb^{85} and Rb^{87}. The relative magnitudes of the signals are correct as shown; but have been displaced vertically so that they coincide at an arbitrary value at $\mathcal{H}=0$.

TABLE III. Comparison of observed hfs constant ratios with ratios of fine-structure intervals. [A reference x/y indicates that reference $x(y)$ was used for the numerator (denominator) of the ratios in columns 4 and 5.]

Atom	n	$\frac{\delta\nu_0(nP)}{\delta\nu_0[(n+1)P]}$	$\frac{a(n\,^2P_{3/2})}{a[(n+1)\,^2P_{3/2}]}$	$\frac{b(n\,^2P_{3/2})}{b[(n+1)^2P_{3/2}]}$	Ref.
Li	2	3.49	3.5 ±0.5		a/b
Na^{23}	3	3.05	3.1 ±0.1	2.4 ±0.3	c/c
K^{39}	4	3.07	3.1 ±0.15	3.2 ±0.3	c/c
Rb^{85}	5	3.066	3.057 ±0.003	3.175 ±0.010	d/e
	6	2.209	2.204 ±0.008	2.23 ±0.05	e/f
	7	1.861	1.87 ±0.02	1.86 ±0.10	f/g
Rb^{87}	5	3.066	3.062 ±0.004	3.185 ±0.015	d/e
	6	2.209	2.204 ±0.003	2.32 ±0.04	e/f
	7	1.861	1.86 ±0.01	1.78 ±0.11	f/g
$Cs^{133,137}$	6	3.061	3.051 ±0.009	3.18 ±0.15	h/i, j/j
	7	2.190	2.178 ±0.002	3 ±3	i/k

[a] B. Budick, H. Bucka, R. J. Goshen, A. Landman, and R. Novick, Phys. Rev. 147, 1 (1966).
[b] R. C. Isler, S. Marcus, and R. Novick, Columbia Radiation Laboratory Progress Report No. 14, 1966 (unpublished)
[c] This work.
[d] H. A. Schussler, Z. Physik 182, 289 (1965).
[e] H. Bucka, H. Kopfermann, and A. Minor, Z. Physik 161, 123 (1961).
[f] H. Bucka, G. zu Putlitz, and R. Rabold, Z. Physik 213, 101 (1968).
[g] G. zu Putlitz and K. V. Venkataramu, Z. Physik 209, 470 (1968).
[h] P. Buck, I. I. Rabi, and B. Senitzky, Phys. Rev. 104, 553 (1956).
[i] H. Bucka, H. Kopfermann, and E. W. Otten, Naturwiss. 45, 620 (1958); H. Bucka, H. Kopfermann, and E. W. Otten, Ann. Physik 4, 39 (1959).
[j] S. Svanberg and S. Rydberg, Z. Physik 227, 216 (1969).
[k] H. Bucka and G. von Oppen, Ann. Physik 10, 119 (1962).

TABLE IV. Comparison of observed hfs constant ratios with predicted scaling law. (Some of the references in this table are listed with Table III).

Atom	State	$\frac{a(^2P_{1/2})}{a(^2P_{3/2})}$ Theory	$\frac{a(^2P_{1/2})}{a(^2P_{3/2})}$ Expt	Refs.
Li^7	2P	5.00	-13.7 ± 1.0	a/b
Na^{23}	3P	5.02	4.96 ± 0.08	c/c
K^{39}	4P	5.09	4.82 ± 0.6	d/e
	5P	5.09	4.56 ± 0.08	f/e
Rb^{85}	5P	5.46	4.77 ± 0.03	g/h
	7P	5.46	4.76 ± 0.02	i/j
Rb^{87}	5P	5.46	4.77 ± 0.05	g/g
Cs^{133}	6P	6.26	5.53 ± 0.02	k/l
	7P	6.26	6.05 ± 0.003	m/n

[a]G. J. Ritter, Can. J. Phys, 43, 770 (1965).
[b]Table III, Ref. a.
[c]M. L. Perl, I. I. Rabi, and B. Senitzky, Phys. Rev. 98, 611 (1955).
[d]P. Buck and I. I. Rabi, Phys. Rev. 107, 1291 (1957).
[e]This work.
[f]G. J. Ritter and G. W. Series, Proc. Roy. Soc. (London) A238, 473 (1957).
[g]B. Senitzky and I. I. Rabi, Phys. Rev. 103, 315 (1956).
[h]Table III, Ref. d.
[i]D. Feiertag and G. Zu Putlitz, Ann. Physik 208, 447 (1968).
[j]Table III, Ref. i.
[k]Ref. 15, p. 101.
[l]Table III, Ref. k.
[m]H. Bucka, Z. Physik 151, 328 (1958).
[n]K. Althoff, Z. Physik 141, 33 (1955).

data, since we could not measure the lamp profile. The excellent fits for Na and K are almost certainly a meaningful verification of the broad-profile assumption. For Rb and Cs, the data used for measuring the lifetimes was taken over a relatively small range of field, so it is reasonable to assume that the magnetic scanning of the beam absorption profile is negligible.

APPENDIX: POSSIBLE OBSERVATIONS OF GROUND-STATE HANLE EFFECT

During the measurements on Rb and Cs, we observed an additional Lorentzian dip at very small magnetic field. Figure 11 shows a typical plot of the experimental data exhibiting this effect. In Fig. 12, we plot typical data obtained by sweeping over a very small range around $\mathcal{H} = 0$. Each of these curves represents several thousand 16-sec sweeps, or integration times of about 1 min for each of 1024 points. The plot for Cs is particularly valuable, since it shows that the dip is very nearly Lorentzian, with a half-width at half-maximum of 0.065 G. The dips for Rb seem to have a small amount of structure for positive magnetic field, indicating that there might have been some more complicated effects contributing. These dips have a half-width at half-maximum of about 0.07 G.

We believe these dips may be due to the Hanle effect in the ground state; i.e., they arise from ground-state pumping as follows: At zero field, the linearly polarized incident light will produce a transverse alignment in the ground state. This alignment modifies the scattered light signal slightly, the amount being proportional to the amount of alignment (which depends on pumping and relaxation rates). As the magnetic field is increased from zero (parallel to the incident light), the transverse alignment will be destroyed and the scattered intensity will change slightly. Similar effects have been discussed by Lehmann and Cohen-Tannoudji, and others.[22]

The field dependence of the scattering rate will be of the form

$$I \sim (1/H^2T)\sin^2 2\pi\gamma HT ,$$

where γ is the gyromagnetic ratio of the ground state

$$\gamma(Rb^{85}) = 0.467 \text{ MHz/G} ,$$

$$\gamma(Cs^{133}) = 0.350 \text{ MHz/G} ,$$

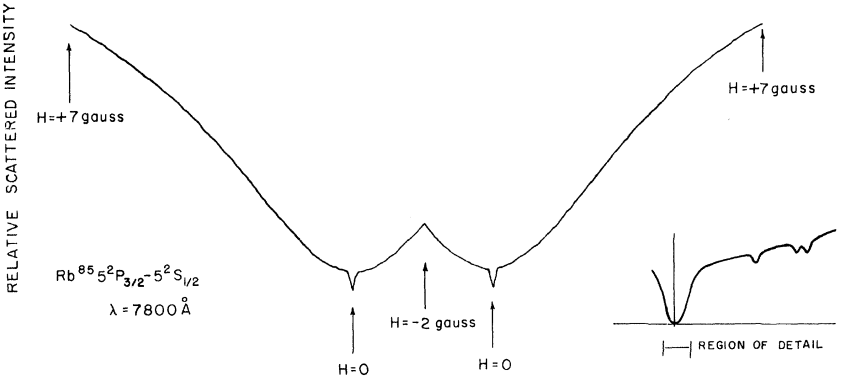

FIG. 11. Rb Hanle-effect line shape exhibiting the very narrow Lorentzian dip at zero field.

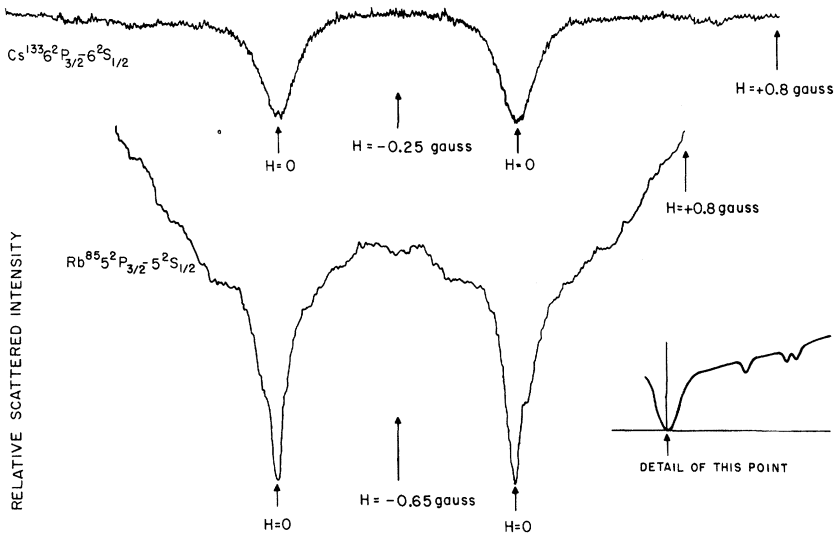

FIG. 12 Possible optical pumping in ground state of Cs (upper curve) and Rb (lower curve) with excitation by first resonance line.

and T is the transit time of the atoms through the light. For path length l and velocity v, we have $T = l/v$. The signal should therefore have a full width at half-maximum (FWHM) $H_{\mathrm{FWHM}} \cong v/\gamma l$.

If we use $v \cong 2\times10^4$ cm/sec, $l \cong 2$ cm (which are typical in our apparatus), we find $H \cong 0.03$ G. This estimate is somewhat smaller but is in reasonable agreement with out data and it should be noted that we have made no allowance for magnetic field inhomogeneity.

This effect was observed in the $5\,^2P_{3/2}$ state of Rb and $6\,^2P_{3/2}$ state of Cs. It was observed repeatedly over several weeks in each case. The apparatus was as described above. We were using lamps of the type shown in Fig. 6(a). There was some evidence that the power input to the lamp affected the magnitude of the dip, but that could not be verified in detail. The width of the dip did not vary appreciably from day to day, but this was not quantitatively investigated.

It is unlikely that the Cs dip could be due to the $7\,^2P_{3/2}$ or $8\,^2P_{3/2}$ states, because the lifetimes of those states are much less than 800 nsec; the lifetime calculated by assuming the observed dip is from Hanle effect in these states. In addition, our interference filter has essentially no transmission at the wavelengths necessary to excite these higher P states.

It is conceivable that the $5\,^2D$ states were being excited either directly (very weak $S \rightarrow D$ transitions have been observed in cesium), or in a two-step excitation process (i.e., $^2S \rightarrow {}^2P \rightarrow {}^2D$), because no filter was used in the input optics. It may be noted that the $5\,^2D_{3/2}$ state has a calculated lifetime of 952 nsec, and its Hanle effect could be observed via cascade through the $6\,^2P$ states. There are several other lines within 600 Å, but it is very unlikely that these could be detected through the interference filter since we measured the transmission of the filter to be much less than 1% for wavelengths more than 150 Å away from 8521 Å. Furthermore, even if the Cs dip is somehow due to the D states, the Rb dip cannot be since the wavelengths and lifetimes are even more disparate.

It is certain that the dips cannot be due to an anomaly in the magnetic field coils or sweeping circuits because the field was swept through the zero by opposing coils, i.e., the current at which zero field occurred varied from run to run.

---

*Work supported in part by the Joint Services Electronics Program (U. S. Army, Navy, and Air Force), under Contract No. DA-28-043 AMC-00099(E) and the U. S. Atomic Energy Commission.

†Present address: Lawrence Radiation Laboratory, University of California, Berkeley, Calif. 94720.

[1]M. Arditi, Ann. Phys. (N. Y.) 5, 973 (1960).
[2]L. Essen, Contemp. Phys. 7, 343 (1966).
[3]W. Happer and E. B. Saloman, Phys. Rev. 160, 23 (1967).
[4]B. S. Mathur, H. Tang, and W. Happer, Phys. Rev. 171, 11 (1968).
[5]J. D. Lyons, R. T. Pu, and T. P. Das, Phys. Rev. 178, 103 (1969).
[6]G. H. Fuller, V. W. Cohen, Nucl. Data Tables U. S. At. Energy Comm. A5, 433 (1969).
[7]R. W. Schmieder, A. Lurio, and W. Happer, Phys. Rev. 173, 76 (1968).
[8]R. W. Schmieder, A. Lurio, and W. Happer (unpublished).
[9]A. Khadjavi, A. Lurio, and W. Happer, Phys. Rev. 167, 128 (1968).

[10]R. W. Schmieder, IBM Res. Rept. RW118, (1969).
[11]G. Breit, Rev. Mod. Phys. 5, 91 (1933); M. E. Rose and R. L. Carovillano, Phys. Rev. 122, 1185 (1961); P. A. Franken, *ibid.* 121, 1508 (1961); H. H. Stroke, G. Fulop, S. Klepner, and O. Redi, Phys. Rev. Letters 21, 61 (1968).
[12]The diagonalization is performed within the manifold of the excited state only, since Eq. (1) is independent of the basis states $|m\rangle$ so long as they span the space of the ground state. That is, $|m\rangle$ enters Eq. (1) only as $\sum|m\rangle\langle m|$ which is invariant in a unitary transformation to another basis.
[13]D. R. Bates and A. Damgaard, Phil. Trans. Roy. Soc. (London) A242, 101 (1949).
[14]O. S. Heavens, J. Opt. Soc. Am. 51, 1058 (1961).
[15]H. Kopfermann, *Nuclear Moments* (Academic, New York, 1958).
[16]G. Sprott and R. Novick, Phys. Rev. Letters 21, 336 (1968); W. E. Baylis, thesis, Munich, 1967 (unpublished); J. Ney, Z. Physik 223, 126 (1969).
[17]R. Sternheimer, Phys. Rev. 80, 102 (1950); 84, 244 (1951); 86, 316 (1953); 95, 736 (1954); 105, 158 (1965).
[18]C. E. Moore, *Atomic Energy Levels*, Natl. Bur. Stds. (U. S.) Circ. No. 467 (U. S. GPO, Washington, D. C., 1949), Vols. I–III.
[19]G. zu Putlitz, Comments At. Mol. Phys. 1, 51 (1969); G. zu Putlitz, Editions du CNRS No. 164, Paris, 1967, p. 205 (unpublished).
[20]E. Fermi, Z. Physik 59, 680 (1930).
[21]A. Gallagher and A. Lurio, Phys. Rev. Letters 10, 25 (1963).
[22]J. Lehmann and C. Cohen-Tannoudji, Compt. Rend. 258, 4463 (1964); A. Kastler, J. Phys. Radium 11, 255 (1950); W. B. Hawkins, Phys. Rev. 98, 478 (1955); P. Franken and F. D. Colgrove, Phys. Rev. Letters 1, 316 (1958).

PHYSICAL REVIEW A VOLUME 2, NUMBER 4 OCTOBER 1970

Contact Transformation and Its Application to the Vibrational Hamiltonian

Fraser W. Birss and Jong H. Choi
Division of Theoretical Chemistry, Department of Chemistry, University of Alberta, Edmonton 7, Alberta, Canada
(Received 28 August 1969; revised manuscript received 21 May 1970)

The criteria for applicability of a full contact transformation are examined. Comments are made on the relation between the Rayleigh-Schrödinger and contact-transformation perturbation representations. The analysis is based upon the use of a Hermitian operator defined as a commutator with the zero-order Hamiltonian and upon the use of the Fock representation. The methods are developed in the context of the vibrational Hamiltonian.

I. INTRODUCTION

From the beginning of the theoretical treatment of vibration-rotation spectra,[1] the primary developments have been based upon the use of perturbation theory. In particular, a contact-transformation scheme, introduced by van Vleck,[2] has been developed[3] and extensively used.[4–7] More recently, Primas[8] has directed attention to the theoretical basis of the method, and Arthurs and Robinson[9] have given some applications. This technique is peculiarly appropriate to vibration-rotation spectra because of the properties, characterized by commutation relations, of the quantum-mechanical operators involved. It is the purpose of this paper to reconsider the mathematical aspects of this application of van Vleck's method by the use of the Fock representation, which proves to be most convenient in this context. The advantage of this representation is best demonstrated when one considers resonance interactions such as the Coriolis and anharmonic resonance interactions. The forms and limitations of the contact transformations are particularly directly obtained by this method.

II. DEGENERATE PERTURBATION THEORY AND CONTACT TRANSFORMATION

We consider a Hamiltonian operator,

$$H=H^{(0)}+V\,,\quad V=\sum_{l=1}H^{(l)}\,, \tag{2.1}$$

where V is the perturbation and the superscript l identifies the order of the perturbation. The zero-order Hamiltonian operator satisfies the relation

$$H^{(0)}\Psi^{(0)}_{i,j}=E^{(0)}_i\Psi^{(0)}_{i,j}\quad (j=1,\ldots,g), \tag{2.2}$$

where the subscript i identifies the eigenvalues and j the degenerate eigenfunctions with common eigenvalue $E^{(0)}_i$. It is assumed that the eigenfunctions are orthonormal. We introduce a contact-transformation operator of the form

$$X=e^{iS}\,, \tag{2.3}$$

with S chosen to be Hermitian, $S=S^\dagger$, so that X is unitary,

$$X^\dagger X=XX^\dagger=1.$$